Solvatochromism and Solvation Dynamics of Structurally Related Cyanine Dyes

Anchi Yu, Catherine A. Tolbert, Darcie A. Farrow, and David M. Jonas*

Department of Chemistry and Biochemistry, University of Colorado, Boulder, Colorado 80309-0215

Received: March 1, 2002; In Final Form: June 14, 2002

Absorption, fluorescence, and magic-angle pump−probe experiments characterize the solvatochromism and relaxation dynamics of three structurally related near-infrared tricarbocyanine dyes (HDITCP, IR125, and IR144) in solution. Agreement with solvatochromic theory is found in solvents where the conductivity approximately matches that predicted for complete ionic dissociation. The nonpolar solvatochromism of HDITCP and IR125 allows the polar solvatochromism of the IR144 absorption spectrum to be attributed to a specific functional group. Resonance structure arguments predict a dipole moment decrease upon electronic absorption by IR144, consistent with the observed solvatochromism. Assuming a point dipole, spherical cavity reaction field model, self-consistent feedback between the solvent and the polarizable IR144 solute accounts for 1/2 to 1/3 of the observed polar solvent shifts. A geometry change in the excited state leads to nearly nonpolar solvatochromism in the IR144 emission spectrum. Femtosecond magic-angle pump−probe transients show similar underdamped intramolecular vibrational quantum beats in all three molecules, but find solvent-dependent overdamped responses on a picosecond time scale in all three dyes. The quantum beat decays determine inhomogeneous vibrational dephasing times of a few picoseconds. Vibrational relaxation, nonpolar solvation, and dielectric relaxation all take place on similar time scales, but the picosecond relaxations are all slower and of larger amplitude for IR144 (polar solvatochromism) than HDITCP (nonpolar solvatochromism). In contrast to HDITCP, IR144 has a prominent solvent-dependent "coherence spike" near $T = 0$ which is attributed to femtosecond polar solvation dynamics.

I. Introduction

Solvation processes play a crucial role in many chemical reactions, and there has been a great deal of interest in understanding both static and dynamic solvent effects.[1−4] The development of femtosecond lasers has allowed direct time-resolved studies of the spectral shifts accompanying charge reorganization upon electronic excitation.[5−18] Charge reorganization is usually accompanied by vibrational displacement and an overall change in molecular size which may occur on similar time scales, so variation of the solute and solvent are required for microscopic insight into the motions observed. One approach has been to study the same solute in different solvents and attribute differences in response to the solvent.[5,8,19] This changes the entire solvent response, polar and nonpolar. An alternative approach varies the solute, and attributes similar responses to the solvent.[3] This assumes the solute probes have no intramolecular response in common. The approach developed here compares structurally related dyes which are sensitive to different solvent properties in a series of solvents. If the responses were independent, this approach would allow a separation of polar solvation from vibrational motion and nonpolar solvation in each solvent. However, simulations indicate that polar and nonpolar solvation are coupled.[20−22] More precisely, such a comparison probes the overall change in the solvation response caused by adding a new polar solute−solvent interaction.

In the absence of specific molecular interactions, the overall solvent dependence of absorption and emission spectra can often be predicted based on continuum electrostatics and Franck−Condon ideas.[23,24] Onsager described the underlying continuum electrostatic theory of a self-consistent solute−solvent "reaction field" for a polar molecule in 1936.[25] Subsequent work has expanded on this idea, sometimes with slightly different assumptions, and found functions of the dielectric constant and refractive index to describe both polar and nonpolar solvatochromism (the solvent dependence of electronic spectra).[1,26,27] All these theories assume the chemical state of the molecule is the same in different solvents and indicate that a polar solvent response requires both a dipole moment and a change in dipole upon electronic excitation. Recent studies of solvation in quadrupolar solvents have found smaller reorganization energies that can have faster inertial solvation time scales (e.g., benzene relaxes faster than acetonitrile).[28,29]

West and Geddes studied the steady-state solvation of several small carbocyanine dyes and found nonpolar solvation.[30] Several groups have used various tricarbocyanine dyes in nonlinear optical experiments to characterize solvation time scales and reached different conclusions about the role of intramolecular and solvent relaxation in the observed signals.[11,31−33] This paper describes comparative studies of the solvatochromism and relaxation dynamics of three structurally related tricarbocyanine dyes: HDITCP, IR125, and IR144. Reasonable agreement with solvatochromic theory is found in solvents where the conductivity approximately matches that predicted for complete ionic dissociation. It is shown here that the linear spectra of these molecules are sensitive to different solvent properties.

It has recently been shown computationally that pump−probe transients can be used to accurately retrieve slow solvation dynamics.[34,35] Magic-angle pump−probe experiments reported here show that the underdamped intramolecular vibrational quantum beats are quite similar in all three molecules, but find

* Corresponding author. Telephone: (303) 492-3818. Fax: (303) 492-5894. E-mail: david.jonas@colorado.edu.

10.1021/jp0205867 CCC: $22.00
Published on Web 09/25/2002

SCHEME 1: Chemical Structures of Tricarbocyanine Dyes HDITCP (a), IR125 (b), and IR144 (c) and Third Resonance Structure for IR144 (d)[a]

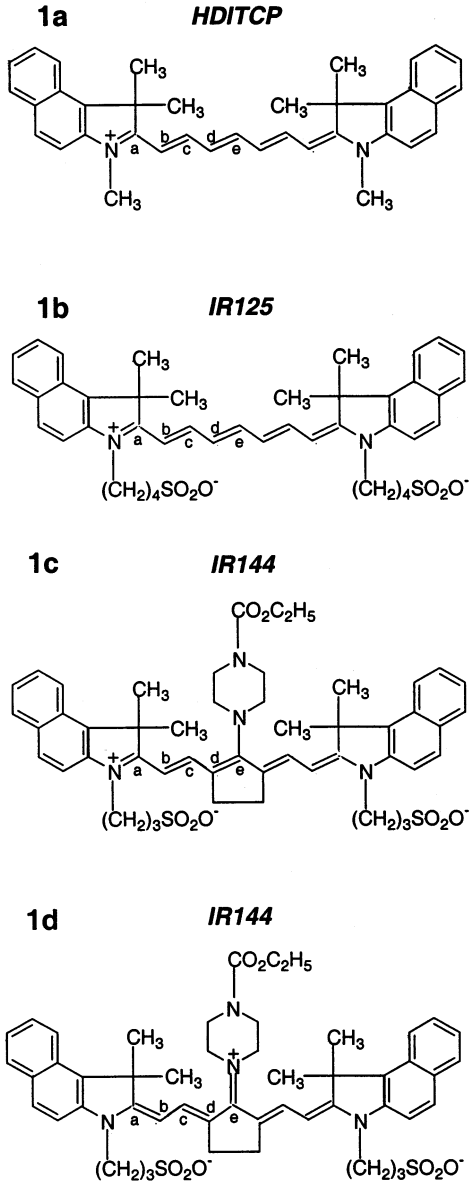

[a] IR125 and IR144 are structurally identical to HDITCP except for the addition of functional groups.

solvent-dependent overdamped and inertial responses in all three dyes. The trends in the time-resolved data are consistent (across both dyes and solvents) with molecular dynamics results.

The chemical structures[36] of the tricarbocyanine dyes HDITCP (Scheme 1a), IR125 (Scheme 1b), and IR144 (Scheme 1c) are shown in Scheme 1. IR125 and IR144 are structurally identical to HDITCP except for the addition of functional groups. Pauling used a two-state valence bond model to explain the lowest allowed electronic transition in all the cyanine dyes as a charge resonance transition between the symmetric and antisymmetric linear combinations of the two mirror image resonance structures with a charge on either N atom.[37] Mulliken explicitly included charge delocalization over the intermediate polymethine chain to account for the spectra.[38,39] With $2n + 4$ π electrons, these dyes have nominally equal bond lengths and charge alternation along the methine chain.[40,41] NMR studies of a carbocyanine in DMSO establish that the charge remains delocalized even in polar solvents on the NMR time scale.[42] The nonpolar solvatochromism of the charge resonance transition (which has been observed for the tricarbocyanine HITCI)[19] establishes that the charge is symmetrically delocalized on a femtosecond time scale.

By analogy, the dipole moment of HDITCP is not expected to change upon electronic excitation. The negatively charged sulfonate groups added to IR125 should produce a large dipole moment, but no change in dipole moment is expected upon electronic excitation because the sulfonate groups are decoupled from the conjugated bonds by the alkyl chain. The central ring structure in IR144 adds rigidity to the polymethine chain and leads to a dipole change upon electronic excitation. In the symmetric ground state, a third resonance structure (Scheme 1d), in which the piperazine nitrogen attached to the center of the polymethine chain donates an electron to the polymethine chain, can increase the dipole moment for IR144. This symmetric resonance structure cannot contribute to the antisymmetric excited state, so the IR144 dipole moment is expected to drop instantly upon electronic excitation. As a result, IR144 exhibits polar solvatochromism. To avoid artificial separation of the IR144 solvent response into polar and nonpolar components, we refer to the entire IR144 response as polar.

II. Theory

The theory of solvatochromism is briefly reviewed here to emphasize the role of solute polarizability. Since the work of Onsager,[25] various workers have proposed different functions of the dielectric constant and refractive index to describe solvatochromism, the solvent-dependent shifts in absorption and emission spectra.[23,24,43−45] The key idea is that the electrons in the solvent will instantly adapt to a new charge distribution upon electronic excitation, while the nuclear degrees of freedom of the solvent will equilibrate only after the electronic excitation in accord with the Franck−Condon principle.[24] The instantaneous electronic response is reflected in the optical refractive index, while the subsequent nuclear relaxation is reflected in the static dielectric constant and far-infrared spectrum. The relative importance of these contributions depends on the solute dipole moment in the ground state, the solute dipole moment change upon electronic excitation, and the change in solute polarizability.

For a polar molecule in a polar solvent, such as IR144 in methanol, forces orient the solvent to stabilize the polar solute. For a polarizable point dipole in a spherical cavity,[25] the ground state (g) dipole moment ($\vec{\mu}_g$) of the solute induces a solvent reaction field ($\vec{E}_g$)

$$\vec{E}_g = \frac{2(D-1)}{2D+1}\frac{(\vec{\mu}_g + \alpha\vec{E}_g)}{a^3}, \tag{1}$$

where D is the solvent dielectric constant, a is the solute radius, and α is the solute polarizability (cgs-Gaussian units are used).

Two approaches to solvatochromism diverge from eq 1. The first neglects the solute polarizability.[26,43,44,46]

$$\vec{E}_g = \frac{2\vec{\mu}_g}{a^3}\frac{D-1}{2D+1}. \tag{2}$$

This is appropriate when the reaction field is too weak to appreciably increase the total solute dipole moment. The second approach assumes an approximate relationship between solvent cavity size and solute molecular polarizability such as $\alpha = (a^3/2)$,[45] which leads to

$$\vec{E}_g = \frac{2\vec{\mu}_g}{a^3}\frac{D-1}{D+2} \quad (3)$$

This approach allows self-consistent feedback between the solvent reaction field and the polarizable solute dipole as in Onsager's model for the dielectric constant of polar liquids.[25] Other proportional relationships ($\alpha = \phi a^3$ with $\phi < 1/2$) between cavity radius and polarizablility have been suggested,[47] and predict slightly different solvatochromism.

To summarize eqs 2 and 3

$$\vec{E}_g = \beta\vec{\mu}_g L(D) \quad (4)$$

where $\beta = 2/a^3$, and

$$L_0(D) = \frac{D-1}{2D+1}$$

or

$$L_{1/2}(D) = \frac{D-1}{D+2}.$$

The ground-state energy is stabilized by

$$U_g = -\vec{\mu}_g \cdot \vec{E}_g = -|\vec{\mu}_g|^2 \beta L(D). \quad (5)$$

When the molecule is electronically excited, its dipole moment and charge distribution will instantly change. The solvent electronic polarization will also instantly adjust, but the solvent configuration (orientations, positions, intramolecular geometries) will not have time to change during the sudden absorption of light. This latter contribution to the solvent polarization, which depends on nuclear positions, is usually called the orientational polarization. Thus, the initial reaction field after electronic excitation has an equilibrium electronic polarization for the excited state but an orientational polarization equilibrated to the ground-state dipole. Before the nuclei can respond, the excited state (e) is affected by two fields:

$$\vec{E}_e{}^0 = \vec{E}_{g,nuc} + \vec{E}_{e,elec} \quad (6)$$

where

$$\vec{E}_{g,nuc} = \beta\vec{\mu}_g[L(D) - L(n^2)] \quad (7)$$

is the reaction field from the orientational polarization alone, and

$$\vec{E}_{e,elec} = \beta\vec{\mu}_e L(n^2) \quad (8)$$

is the field from the electrons.[48] The initial (Franck−Condon) stabilization of the excited state is thus

$$U_e = -\vec{\mu}_e \cdot (\vec{E}_{g,nuc} + \vec{E}_{e,elec}) = -\beta\vec{\mu}_e\vec{\mu}_g[L(D) - L(n^2)] - \beta|\vec{\mu}_e|^2 L(n^2). \quad (9)$$

The solvent shift in absorption wavenumber is thus $\Delta\nu_{abs} = (U_e - U_g)/hc$, so that

$$\nu_{abs} = \nu_a{}^0 + \beta'\vec{\mu}_g \cdot (\vec{\mu}_g - \vec{\mu}_e)[L(D) - L(n^2)] + \beta'(|\mu_g|^2 - |\mu_e|^2)L(n^2), \quad (10)$$

where $\beta' = \beta/hc$, and $\nu_a{}^0$ is nominally a gas phase (solvent-free) absorption frequency.[41] The term proportional to $[L(D) - L(n^2)]$ arises from the slow orientational solvent polarization while the term proportional to $L(n^2)$ arises from the instantaneous electronic polarizability. A similar analysis beginning with the solvent equilibrated to the excited state yields a solvent shift in the emission wavenumber

$$\nu_{em} = \nu_e{}^0 + \beta'\vec{\mu}_e \cdot (\vec{\mu}_g - \vec{\mu}_e)[L(D) - L(n^2)] + \beta'(|\mu_g|^2 - |\mu_e|^2)L(n^2). \quad (11)$$

Note that the orientational polarization dependence of the emission spectrum differs from the absorption spectrum because the initial conditions determine the solvent configuration after the transition. In contrast, the electronic polarization dependence is the same because it instantly adapts during the transition. If $\vec{\mu}_g \parallel \vec{\mu}_e$ and $|\vec{\mu}_g| > |\vec{\mu}_e|$, as expected for IR144, both the absorption and fluorescence shift to the blue with increasing solvent polarity, but the absorption shifts are greater. The solvent dependence of the Stokes shift is given by

$$\nu_{abs} - \nu_{em} = 2\lambda = \beta'|\vec{\mu}_g - \vec{\mu}_e|^2[L(D) - L(n^2)] \quad (12)$$

and depends only on the orientational polarization.

Equations 10−12 indicate that a large dipole moment and a change in dipole moment are both required for polar solvatochromism. Neglecting solute polarizability, the orientational solvent polarity is characterized by

$$F_0(D,n) = L_0(D) - L_0(n^2) = \frac{D-1}{2D+1} - \frac{n^2-1}{2n^2+1}, \quad (13)$$

where n is the refractive index and D is the dielectric constant for the solvent.[26,43,44,46] The approximation $\alpha = (1/2)a^3$ yields

$$F_{1/2}(D,n) = L_{1/2}(D) - L_{1/2}(n^2) = \frac{D-1}{D+2} - \frac{n^2-1}{n^2+2}. \quad (14)$$

Following Marcus,[5,49−51] some works have also considered the solvent dependence of the spectral width, specified by the variance σ^2. Assuming harmonic potentials of equal curvature, the classical Franck principle (which assumes the Condon approximation) relates σ^2 to the Stokes shift $\nu_{abs} - \nu_{em} = 2\lambda$ by

$$\sigma^2 = 2\lambda(k_B T/hc), \quad (15)$$

where σ and λ are in wavenumbers. With these assumptions, the widths of the emission and absorption spectra are predicted to be the same. Equation 15 need not hold if high-frequency vibrations ($\hbar\omega > k_B T$) are important for the band shape,[49−51] but the mirror image symmetry remains in the harmonic approximation. The additivity of Gaussian variances under convolution leads to $\delta(\sigma^2) = 2(\delta\lambda)(k_B T/hc)$ where $\delta(\sigma^2)$ and $\delta\lambda$ are the solvent-induced changes in the variance and Stokes shift, respectively.[5]

Previous experimental and theoretical studies have shown that pump−probe transients are sensitive to the solvation dynamics because shifts in the time-evolving molecular spectra change their overlap with the probe spectrum.[8,31,34,35,52] In the high-temperature Brownian oscillator model, the frequency−frequency correlation function $M(t)$ can be used to calculate the pump−probe signal. For conditions similar to our experiments (Stokes shift ∼100−500 cm^{-1}, excitation midway between absorption and emission maxima, 30 fs pulse), we have found that a single picosecond exponential decay in $M(t)$ leads to a pump−probe transient that can be well fit as biexponential decay, with the slowest time constant within ±10% of the input

single-exponential decay $M(t)$ time constant. The faster decay has very roughly one-third the time constant and one-fourth the amplitude.[35] Assuming the Brownian oscillator model, the slowest time scales accurately reflect the solvation dynamics. These conclusions are not modified by inclusion of much faster relaxation processes.[34,35] Dielectric continuum theory, which is most likely to succeed for the slowest processes, predicts that the reaction field, hence $M(t)$, will relax exponentially with longitudinal relaxation times which depend weakly on the solute polarizability.[53]

Nonpolar solvatochromism is usually described by a "general red shift" attributed to dispersion interactions with the solvent.[1,23]

$$\nu_{abs} = \nu_a^0 - \gamma L_0(n^2) \tag{16}$$

$$\nu_{em} = \nu_e^0 - \gamma L_0(n^2) \tag{17}$$

where γ is the same for both absorption and emission because the electrons adjust instantaneously during the transition. This should be present for all solute−solvent systems, though it may be masked by polar solvation. Longuett-Higgins and Pople[54] have proposed that the "general red shift" is proportional to solvent polarizability. The Clausius−Mossoti equation[55] indicates that the slightly different function $L_{1/2}(n^2)$ is proportional to the solvent polarizability. With different approximations, the dispersion interaction has been interpreted in terms of transition dipole solvation,[23] changes in solute polarizability upon electronic excitation,[1] and as a sum of a universal and an oscillator strength dependent shift.[54] The general red shift can be partly canceled by a blue shift (relative to gas phase) due to mechanical solvent caging of the larger electronically excited molecules.[56,57] Bernstein and co-workers have argued that a lack of mirror image symmetry in various cryogenic solvents is caused by such anharmonic solute−solvent potentials.[58] Theories of nonpolar vibrational frequency shifts which incorporate both attractive and repulsive packing forces have been developed.[59] We are not aware of a theory of nonpolar electronic solvatochromism which consistently incorporates both attractive dispersion forces and repulsive solvent caging. However, the viscoelastic theory of the subsequent nonpolar solvation dynamics is well developed.[13]

With two definitions of $L(x)$ and polar/nonpolar formulas, there are four possible functions to describe the solvatochromic shifts. From here on they will be referred to as $F_0(D,n)$, $F_{1/2}(D,n)$, $f_0(n)$, and $f_{1/2}(n)$. Capital F refers to polar functions; lowercase f refers to nonpolar functions. Subscript 1/2 indicates $L_{1/2}(x)$ is used for both $x = D$ and $x = n^2$.

$$f_0(n) = \frac{n^2 - 1}{2n^2 + 1}, \tag{18a}$$

$$f_{1/2}(n) = \frac{n^2 - 1}{n^2 + 2}, \tag{18b}$$

$$F_0(D,n) = \frac{D - 1}{2D + 1} - \frac{n^2 - 1}{2n^2 + 1}, \tag{19a}$$

$$F_{1/2}(D,n) = \frac{D - 1}{D + 2} - \frac{n^2 - 1}{n^2 + 2}. \tag{19b}$$

All four of these functions have been used in the literature of solvatochromism.[5,23,26,30,43,44,60,61] The functions in eqs 18 and 19 were calculated from refractive indices and dielectric constants and are listed in Table 1. $f_0(n)$ and $f_{1/2}(n)$ are highly correlated (correlation coefficient = 0.9996) for the solvents used here. $F_0(D,n)$ and $F_{1/2}(D,n)$ are less correlated (correlation coefficient = 0.88, which is less than expected for two sorted sets of uniformly distributed random numbers).

TABLE 1: Solvatochromism Functions for Solvents Used in These Experiments, Calculated from Refractive Indices (n) from Ref 66 and Dielectric Constants (D) from Ref 5

solvent	$f_0(n)$	$f_{1/2}(n)$	$F_0(D,n)$	$F_{1/2}(D,n)$
methanol	0.1690	0.2033	0.3084	0.7101
acetonitrile	0.1749	0.2120	0.3045	0.7090
ethanol	0.1812	0.2213	0.2889	0.6657
1-propanol	0.1899	0.2343	0.2743	0.6320
1-butanol	0.1949	0.2420	0.2635	0.6042
propylene carbonate	0.2016	0.2525	0.2870	0.7027
ethylene glycol	0.2059	0.2593	0.2745	0.6652
formamide	0.2109	0.2673	0.2824	0.7062
acetone	0.1804	0.2200	0.2840	0.6470
benzonitrile	0.2357	0.3084	0.2351	0.5813

III. Experimental Section

The three dyes were each tested in 20 different solvents.[62] A number of solvents (diiodomethane, 1-octanol, glycerin, cyclohexane, trichlorotrifluoroethane) did not dissolve the dyes. Some precipitated dye, leaving a colorless solution a few hours after removal from the ultrasound (e.g., HDITCP in benzene). Some (e.g., IR125 in water) had concentration-dependent spectra characteristic of aggregates[63] at the concentrations needed for nonlinear experiments. IR144 in water produced a double-peaked absorption spectrum, apparently independent of concentration down to 10^{-7} M. IR144 in acetone produced a double-peaked emission spectrum. Changes in width were observed upon addition of 1% methanol to HDITCP in chloroform. Solutions of IR144 in chloroform with 0.1% amylenes as stabilizer (Aldrich) had an absorption maximum 5 nm to the blue of IR144 in chloroform with 0.75% ethanol stabilizer (Fisher). Because of this preferential solvation, procedures which use 1% methanol to dissolve cyanine dyes in nonpolar solvents[30] were avoided. Acetone, formamide, ethylene glycol, 1-butanol, and acetonitrile were Fisher standard grade solvents, anywhere from 98% to 99.9% pure. Methanol was Fisher HPLC grade with ≥99.9% purity. Ethanol (anhydrous), 1-propanol, propylene carbonate (anhydrous), and benzonitrile were Aldrich HPLC grade with less than 0.01% water.

Cyanine dyes form ion pairs in low-polarity solvents.[64] Conductance measurements were performed on the solutions at a concentration of approximately 0.04 mM using a digital conductance meter (Cole Parmer 1481-61) and a platinum probe with a cell constant of 10 cm^{-1}.[65] The *apparent* Walden product ($\Lambda\eta$) of the measured molar conductivity (Λ) at 0.04 mM and viscosity (η) from the CRC Handbook[66] was compared to the Walden product calculated assuming complete dissociation[67] to roughly determine whether the dye dissociated into ions at the concentrations used for nonlinear spectroscopy. There has been some doubt about the utility of the Walden product, especially for small ions,[68] where solvation shells are important. The sodium counterion for IR125 is small, so the radius was taken from a transport calculation for water.[69]

There were some clear rejects with less than 10% of the expected conductivity change (all three dyes in chloroform and benzene, IR125 in 1-propanol, dibromomethane, and benzonitrile, IR144 in dichloromethane and dibromomethane), but any solvent with an apparent Walden product less than 40% of the expected product was deemed suspect (IR144 in benzonitrile and acetone, IR125 in acetonitrile, dichloromethane, and acetone). The spectra of HDITCP in benzonitrile and dichlo-

romethane (which may form ion pairs for the other dyes) exhibited anomalous solvatochromism and also were not used in fitting the solvatochromism.

Application of solvatochromic theory also requires that the spectrum arise from one solute isomer. In low-polarity solvents, some cyanines (e.g., DTTC Chloride) exist as a mixture of cis and trans isomers.[70] To determine polymethine chain conformation, one- (1D) and two-dimensional (2D) COSY proton nuclear magnetic resonance spectra[71] were recorded on a 500 MHz spectrometer for all three dyes in perdeuteromethanol (1 mg/mL) at room temperature. Assignments of the polymethine protons were straightforward based on the multiplet structures, areas, and 2D COSY cross-peaks. The polymethine proton resonances are reported in the following form:

(polymethine carbon as labeled in Scheme 1)
chemical shift δ (number of protons H)
*d*oublet or *t*riplet, $^3J_{HH}$ spin−spin coupling constant

HDITCP: (b) 6.32 ppm δ (2H) *d*, $J = 13.6$ Hz; (c) 8.05 ppm δ (2H) *t*, $J = 13.1$ Hz*; (d) 6.59 ppm δ (2H) *t*, $J = 12.6$ Hz; (e) 7.66 ppm δ (1H) *t*, $J = 13$ Hz*. IR125: (b) 6.39 ppm δ (2H) *d*, $J = 13.5$ Hz; (c) 8.04 ppm δ (2H) *t*, $J = 12.9$ Hz*; (d) 6.63 ppm δ (2H) *t*, $J = 12.2$ Hz; (e) 7.66 ppm δ (1H) *t*, $J = 13$ Hz*. IR144: (b) 6.01 ppm δ (2H) *d*, $J = 13.2$ Hz; (c) 7.91 ppm δ (2H) *d*, $J = 13$ Hz*. (Asterisks indicate a multiplet overlapped by aromatic protons with *J* determined from 2D COSY. A unique assignment for IR144 relies on comparison to HDITCP and IR125.) Protons at symmetry-related positions for the all-trans structure are equivalent and all spin−spin couplings are $^3J_{HH} = 13.1$ Hz within ±0.5 Hz. Assuming $^3J_{HH} = 13$ Hz for trans, the Karplus equation[72,73] predicts $^3J_{HH} \approx 8$ Hz for the cis geometry (as observed for the aromatic protons). In conformational studies, couplings of $^3J_{HH} \simeq 13$ Hz have previously been reported to indicate quasi-planar all-trans cyanine structures.[74−76] The proton chemical shifts are qualitatively consistent with the charge alternation expected for polymethines.[40,41] All three samples contained impurities (or minor forms with millisecond lifetimes) below the 2% level.

Absorption spectra were taken using a Varian Cary 500 UV−vis−NIR spectrometer. Concentrations ranged from 0.05 to 0.1 mM. The molar extinction coefficient $\epsilon(\nu)$ reflects some electromagnetic aspects of absorption in addition to the Franck−Condon intensity envelope, so the spectra were converted to the product of the Einstein *B* coefficient and a normalized absorption line shape function $g_a(\nu)$[77]

$$Bg_a(\nu) = \frac{1000\ (\mathrm{cm^3/L})\ \ln(10) c}{N_A h} \frac{\epsilon(\nu)}{\nu} \propto \frac{\epsilon(\nu)}{\nu} \qquad (20)$$

This normalized line shape function $g_a(\nu)$ reflects the Franck−Condon intensity envelope in the theories of solvatochromism.

Fluorescence spectra were measured by excitation with a 1 mW continuous wave He−Ne laser ($\lambda = 632.8$ nm), which was focused to less than 1 mm diameter and sent through the sample cell within ~1 mm of the collection window. Dye concentrations were around 10^{-7} M, and it was verified that the raw fluorescence spectra were concentration independent below 10^{-5} M. The sample flow rate was 0.2 m/s. The fluorescence was collected perpendicular to the beam path, filtered by either an absorbing Schott RG665 filter or a 632 nm dichroic Raman notch filter, focused by a 5X microscope objective into a multimode fiber, dispersed by a 0.25 m imaging spectrograph, and detected with a liquid nitrogen cooled CCD array. The wavelength resolution was 0.3 nm. For the fluorescence, the frequency axis was calibrated with an argon lamp (Oriel 6030). Intensities were corrected with a calibrated quartz−tungsten−halogen lamp (Oriel 63355) spectrum measured using the same filter, objective, fiber, spectrograph, and range of CCD pixel integration. Combining all corrections, the emission line shape function is

$$Bg_e(\nu) \propto F(\lambda = c/\nu)\ \mathrm{IC}(\lambda = c/\nu)/\nu^6 \qquad (21)$$

where $F(\lambda = c/\nu)$ is the fluorescence spectrum detected by the CCD array in counts/pixel, IC($= c/\nu$) is the intensity correction factor in (watts/nm)/(counts/pixel), and $1/\nu^6$ comes from multiplication of (1) the Jacobian transformation from even wavelength to even frequency intervals ($1/\nu^2$),[78] (2) the conversion from watts to photons per second ($1/\nu$), and (3) the conversion from Einstein *A* to Einstein *B* coefficient ($1/\nu^3$).[77]

For study of spectral relaxation dynamics (e.g., solvation), integrated magic-angle pump−probe experiments were carried out using detection identical to that in ref 79 except that the 1.117 kHz chopper was not phase-locked to the cavity dumped laser. Pulses from a 10 kHz cavity dumped femtosecond Ti:sapphire laser were sent through a prism compressor with LaKL21 prisms and split into three beams: one for the pump beam, one for the probe beam, and the third for the reference beam. The pump was vertically polarized by an antireflection coated Polarcor polarizer (Newport 05P109AR.16). The probe was polarized by a nominally identical polarizer. The probe polarization was rotated to the magic angle (within 0.5°) by a zero-order half-waveplate (Optics for Research RZ-1/2-800) immediately before the 10 cm focal length achromat which focused the pump and probe into the sample. The pulses were characterized with second harmonic generation frequency resolved optical grating (SHG FROG) by substituting a thin KDP wedge glued to the back of a 1 mm fused silica window for the sample cell (which has 1 mm thick fused silica walls). The pulse spectra were approximately Gaussian with a 36 nm wide spectrum centered at 795 nm. The pulses had a 30 fs time duration, and a fwhm time bandwidth product $\Delta\nu\Delta t = 0.490$, larger than the Gaussian transform limit of 0.441. The probe pulse energy was set around 150 pJ/pulse, and the pump pulse energy was set about 250 pJ/pulse in a 40 μm diameter spot. The sample concentration was about 0.07 mM ($OD_{max} \simeq 0.1$ at 750 nm). The antireflection coated sample cell had a 100 μm path length through which sample flowed at a linear speed of 2 m/s. The signal:noise ratio of the pump−probe signals is higher than 200:1. Time zero was determined to within 1 fs using symmetry upon interchange of the roles between pump and probe beams. Delay stage misalignment caused a 15% reduction in probe transmission through a 30 μm pinhole over the range −2 ps to 1.1 ns, so the pump−probe signals were divided by the smoothed delay dependent probe transmission. A rough study of the signal concentration dependence suggests the small negative dip (1% of maximum signal) observed before time zero in the pump−probe signal could be eliminated by decreasing the sample concentration.

IV. Results

Figure 1 shows the absorption and emission line shape functions of HDITCP (Figure 1a), IR125 (Figure 1b), and IR144 (Figure 1c) in methanol. From Figure 1a, HDITCP does not have mirror image symmetry, with emission line shape slightly (~70 cm^{-1}) narrower than absorption. The weak band near 14 200 cm^{-1} in the fluorescence spectrum has the same width

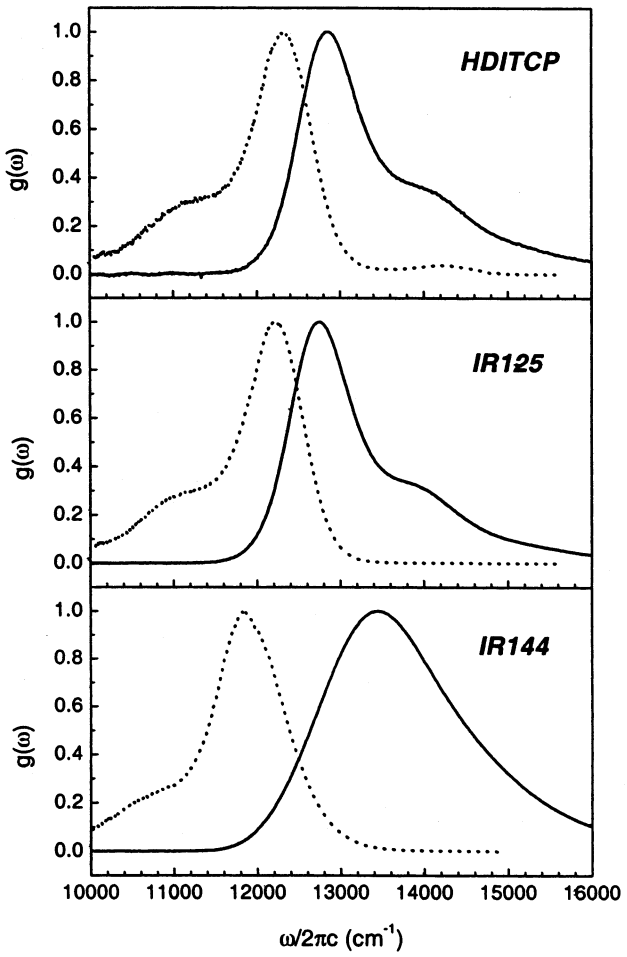

Figure 1. Absorption (solid line) and emission (dotted line) line shape functions of HDITCP (top), IR125 (middle), and IR144 (bottom) in methanol. Line shape functions are normalized to $g_{max} = 1$.

as the main emission band and a solvent- and temperature-dependent intensity. (The Raman notch filter was used to rule out fluorescence from the absorbing filter as the cause of this band.) This HDITCP emission band lies 1900 cm^{-1} above the main emission band and could arise from emission by vibrationally hot molecules, isomers, or impurities with a much larger absorption cross section than normal HDITCP at 632 nm. IR125 is similar to HDITCP, but does not show the 14 200 cm^{-1} emission band and obeys a closer mirror image relation. The closer mirror image symmetry in IR125 argues that the shoulder near 14 200 cm^{-1} in the HDITCP absorption spectra is vibrational (vibrational frequency ~1300 cm^{-1}). Mulliken assigned similar shoulders observed in a series of polyenes to CC stretch vibrations and explained how low-frequency deformations of a planar polyene chain could account for the remaining Stokes shift and broadening.[38,39] The vibrational quantum beat at 1310 cm^{-1} reported by Yang et al.[80] supports this assignment.[81] IR144 has a rather severe departure from mirror image symmetry in all solvents studied.

The absorption maxima, emission maxima, Stokes shifts, full widths at half-maxima, and absorption variances σ^2 for HDITCP, IR125, and IR144 are presented in Tables 2, 3, and 4, respectively. The full widths at half-maxima are heavily influenced by the ~1300 cm^{-1} vibrational shoulder. For comparison to theories of solvent broadening (which do not explicitly include vibrational structure), the variance of the absorption spectrum σ^2 is calculated from the full width at three-fourths maximum ($\Gamma_{3/4}$) using the Gaussian relation

$$\sigma^2 = \Gamma_{3/4}{}^2/[8 \ln(4/3)] \tag{22}$$

Previous studies[5,49−51] have used similar procedures[50] to show that the width of an absorption spectrum with polar solvatochromism depends on the orientational solvent polarity according to eq 15.

In attempting to determine which solvent function best predicted the behavior of HDITCP, IR125, and IR144, the absorption maxima, emission maxima, Stokes shifts, and absorption σ^2 were each fit to all four solvatochromism functions. The best linear least squares fits are shown in Figures 2−4. The fit parameters are listed in Tables 5−7.

The fit errors show that HDITCP and IR125 can be fit by either of the highly correlated nonpolar functions $f_0(n)$ or $f_{1/2}(n)$, while IR144 is best described by the polar function $F_{1/2}(D,n)$. For HDITCP and IR125, the polar F functions do not fit the data (the standard fit errors are 2−3 times larger than that for nonpolar f functions when fitting absorption and emission maxima). The Stokes shift and width parameters were independent of solvent within error for both dyes, as expected for instantaneous electronic solvation. The variance and Stokes shift do not obey eq 15, indicating that high-frequency vibrations (known from Raman[82] and pump−probe experiments[19] on similar molecules) which require a quantum treatment are important for the shape of the main peak near the maximum.[49−51] Constraining the absorption and emission slopes to be the same yields, $\nu_0 = 13\,466$ cm^{-1}, $2\lambda_{0,HDITCP} = 540$ cm^{-1}, and $\gamma = -3003$ cm^{-1} vs $f_{1/2}(n)$ in eqs 16 and 17. These trends for both HDITCP and IR125 are consistent with the work of West and Geddes,[30] who found a general polarizability red shift for a number of smaller cyanine dyes. The slope of the absorption maximum vs the refractive index function $f_0(n)$ or $f_{1/2}(n)$ is about 80% of that observed by West and Geddes for smaller cyanine dyes, and indicates nonpolar solvation.

Intramolecular factors being equal, there will be a larger Stokes shift between the absorption and fluorescence when the dipole changes. IR144 consistently has a larger Stokes shift than HDITCP and IR125, consistent with a dipole change upon electronic excitation. For the absorption (fluorescence) maxima of IR144, the polar F functions had 6 times (2 times) less fit error than the nonpolar f functions. Bilinear fits to both polar and nonpolar functions did not recover a significant nonpolar dependence. Based on eqs 10 and 11, the absence of a significant nonpolar coefficient suggests that the aklylsulfonate chains may be bent out of the conjugated aromatic/polymethine plain so that $\vec{\mu}_g$ is not parallel to $\vec{\mu}_e$. Alternatively, this could result from a cancellation of mechanical and polarizability terms (see discussion below eq 17) connected to the polar solvent interaction. For absorption, the fit to $F_{1/2}(D,n)$ had 3 times lower fit error than that to $F_0(D,n)$. This significantly improved fit from a polarizable solute model suggests that feedback between solvent reaction field and solute polarizability is important for the equilibrium solvation of IR144. For IR144, the solvent change in absorption variance and Stokes shift obey the relation

$$\frac{\partial(\sigma^2)}{\partial F_{1/2}} = \left(\frac{\partial(2\lambda)}{\partial F_{1/2}}\right) k_B T/hc \tag{23}$$

within error. Such a relation is expected if the solvent contribution to the broadening obeys eq 15.[5,50] The extrapolation of σ^2 back to $F_{1/2} = 0$ yields a variance which is consistent (within very large error) with that of HDITCP and IR125 (see Tables 5−7). The 660 cm^{-1} width of the IR144 absorption line shape at a nonpolar interface[83] is slightly less than the raw 980 cm^{-1}

TABLE 2: Absorption Maxima, Emission Maxima, Stokes Shift, Full Widths at Half-Maxima, and Absorption σ^2 for HDITCP in Various Solvents, from Experimental Line Shape Functions $g_{abs}(\omega)$ and $g_{em}(\omega)$

solvent	abs max (cm^{-1})	em max (cm^{-1})	Stokes shift (cm^{-1})	abs fwhm (cm^{-1})	em fwhm (cm^{-1})	abs σ^2 [$(cm^{-1})^2$][a]
methanol	12 853	12 320	533	1000	864	148 699
acetonitrile	12 838	12 291	547	1073	836	164 341
ethanol	12 788	12 213	575	970	868	144 159
1-propanol	12 744	12 216	528	952	864	146 168
1-butanol	12 719	12 186	533	963	863	143 659
propylene carbonate	12 747	12 200	547	1022	854	145 162
ethylene glycol	12 700	12 190	510	957	899	140 183
formamide	12 681	12 145	536	968	866	142 164
acetone	12 816	12 259	557	1016	856	149 208
benzonitrile	12 509	11 975	534	957	828	145 665
error	±20	±20	±30	±30	±30	±20 000

[a] Calculated using eq (22).

TABLE 3: Absorption Maxima, Emission Maxima, Stokes Shift, Full Widths at Half-Maxima, and Absorption σ^2 for IR125 in Various Solvents, from Experimental Line Shape Functions $g_{abs}(\omega)$ and $g_{em}(\omega)$

solvent	abs max (cm^{-1})	em max (cm^{-1})	Stokes shift (cm^{-1})	abs fwhm (cm^{-1})	em fwhm (cm^{-1})	abs σ^2 [$(cm^{-1})^2$][a]
methanol	12 750	12 217	533	961	951	144 660
ethanol	12 694	12 138	556	936	864	139 197
1-butanol	12 617	12 114	503	1020	873	157 467
propylene carbonate	12 645	12 129	516	978	835	144 159
ethylene glycol	12 619	12 125	494	909	875	136 262
formamide	12 607	12 104	503	936	846	150 740
error	±20	±20	±30	±30	±30	±20 000

[a] Calculated using eq (22).

TABLE 4: Absorption Maxima, Emission Maxima, Stokes Shift, Full Widths at Half-Maxima, and Absorption σ^2 for IR144 in Various Solvents, from Experimental Line Shape Functions $g_{abs}(\omega)$ and $g_{em}(\omega)$

solvent	abs max (cm^{-1})	em max (cm^{-1})	Stokes shift (cm^{-1})	abs fwhm (cm^{-1})	em fwhm (cm^{-1})	abs σ^2 [$(cm^{-1})^2$][a]
methanol	13 447	11 838	1609	1909	983	581 653
acetonitrile	13 519	11 855	1664	1955	1011	605 008
ethanol	13 257	11 771	1486	1875	958	563 696
1-propanol	13 151	11 747	1404	1826	965	535 357
1-butanol	13 082	11 731	1351	1794	989	524 799
propylene carbonate	13 438	11 798	1640	1956	1036	605 008
ethylene glycol	13 317	11 786	1531	1886	1103	570 646
formamide	13 427	11 803	1624	1877	1082	550 902
error	±20	±20	±30	±30	±30	±45 000

[a] Calculated using eq (22).

width of the HDITCP line shape (see Table 2). However, the extrapolated IR144 Stokes shift at $F_{1/2} = 0$ is negative or zero, and the emission widths are all ~2 times narrower than absorption (see below).

Magic-angle pump−probe transients of IR144 and HDITCP were recorded in several solvents. Figure 5 shows the magic-angle pump−probe transients of HDITCP and IR144 in methanol. For comparison, the plots are normalized to have the same amplitude for the population lifetime. With this normalization, HDITCP, IR125, and IR144 have very similar quantum beat amplitudes and frequencies. Compared to HDITCP and IR125, IR144 has a much bigger "coherence spike" near $T = 0$. This spike is solvent dependent and is thus attributed to solvation. The Fourier transform (FT) power spectra of HDITCP and IR144 are also shown in the inset to Figure 5. Although comparison of amplitude in the FT can be complicated by interference from the decaying background (which was subtracted prior to the FT to minimize this effect), the dominant frequencies recovered from the quantum beats are very similar. The exponential decay time of the quantum beats range from 1 to 5 ps, in good agreement with previous measurements.[8,80] The recovered vibrational frequencies and dephasing times vary from solvent to solvent, apparently due to specific interactions as observed by Raman[4] and infrared[41] spectroscopies on various molecules.

Magic-angle pump−probe scans extending to 1.1 ns pump−probe delay were fit to a sum of two or three exponential decays starting at 500 fs. Estimates of the reduced chi squared χ_ν^2 ranged from 0.987 to 1.10. The decay times and amplitudes are given in Tables 8 and 9. The slowest decays (400−800 ps) reflect the population lifetime as measured by either transient excited-state absorption[84] or fluorescence.[85] For IR144, the faster decay times roughly parallel picosecond decays attributed to solvation in the three pulse echo peak shift.[8,11] However, there is an apparently significant increase (0.05−0.21) in χ_ν^2 if the decay times are constrained to match the three pulse echo data and a significant increase (>0.5) if the amplitudes are also constrained. The relationship between the IR144 and HDITCP decay times and amplitudes will be discussed below.

V. Discussion

Static Solvatochromism. The linear spectra show that HDITCP and IR125 exhibit classic nonpolar solvatochromism.[30] Such nonpolar solvatochromism was also found in the tricarbocyanine dye HITCI.[19,86] The absorption spectra of IR144 show polar solvatochromism. Both absorption shifts and widths are

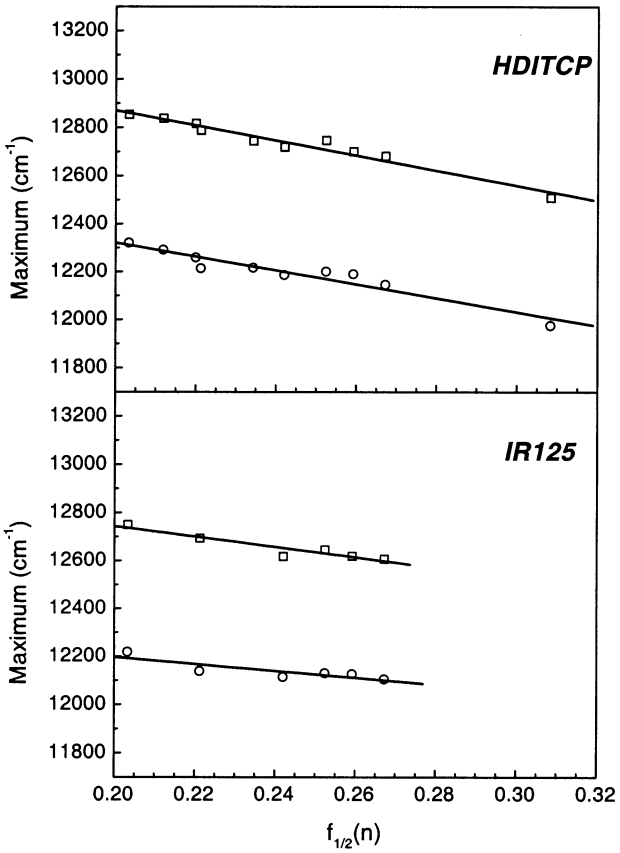

Figure 2. The best linear least squares fits (solid line) to the experimental absorption maxima (open squares) and fluorescence maxima (open circles) vs $f_{1/2}(n)$ for HDITCP (top) and IR125 (bottom).

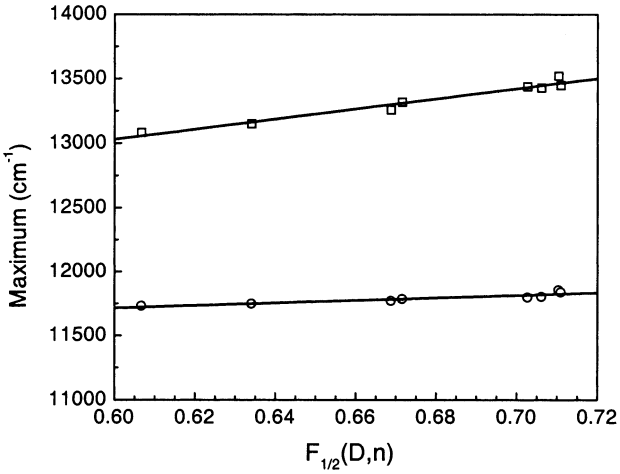

Figure 3. The best linear least squares fits (solid line) to the experimental absorption maxima (open squares) and fluorescence maxima (open circles) vs $F_{1/2}(D,n)$ for IR144.

consistent with a reduction in IR144 permanent dipole upon electronic excitation.

However, the widths of the IR144 emission spectra show a severe departure from mirror symmetry and do not seem to reflect the full solvent contribution to the absorption width. The IR144 emission maxima have a weak solvent dependence and can be fit to $f_{1/2}$ nonpolar solvatochromism with a doubled fit error. Nonpolar solvatochromism would imply that the emitting state either does not have a permanent dipole or does not have a permanent dipole change *during* emission. In the antisymmetric excited state, the piperazine nitrogen attached to the

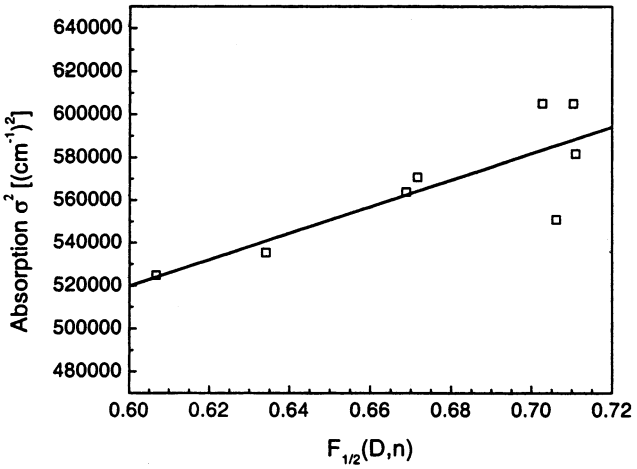

Figure 4. The best linear least squares fit (solid line) to the experimental absorption σ^2 (open squares) vs $F_{1/2}(D,n)$ for IR144.

TABLE 5: Fitting Data for HDITCP[a]

	Y-intercept	slope	std error
abs max (cm^{-1})	13 493 (58)	−3 112 (237)	22
em max (cm^{-1})	12 901 (74)	−2 898 (303)	28
Stokes shift (cm^{-1})	540 (35)	*b*	13
abs σ^2 [(cm^{-1})^2]	146 941 (17 401)	*b*	5 022

[a] The absorption maxima, emission maxima, Stokes shift, and absorption σ^2 were fitted to $f_{1/2}(n)$, and the slopes, *Y*-intercept, and errors are reported here. [b] Constrained to zero because not significantly different.

TABLE 6: Fitting Data for IR125[a]

	Y-intercept	slope	std error
abs max (cm^{-1})	13 177 (94)	−2 166 (388)	21
em max (cm^{-1})	12 482 (104)	−1 429 (428)	23
Stokes shift (cm^{-1})	518 (39)	*b*	25
abs σ^2 [(cm^{-1})^2]	145 414 (12 053)	*b*	8 634

[a] The absorption maxima, emission maxima, Stokes shift, and absorption σ^2 were fitted to $f_{1/2}(n)$, and the slopes, *Y*-intercept, and errors are reported here. [b] Constrained to zero because not significantly different.

TABLE 7: Fitting Data for IR144[a]

	Y-intercept	slope	std error
abs max (cm^{-1})	10 757 (218)	3 815 (323)	34
em max (cm^{-1})	11 140 (119)	964 (176)	19
Stokes shift (cm^{-1})	−384 (157)	2 850 (233)	25
abs σ^2 [(cm^{-1})^2]	162 475 (120 954)	600 049 (179 083)	18 992

[a] The absorption maxima, emission maxima, Stokes shift, and absorption σ^2 were fitted to $F_{1/2}(D,n)$, and the slopes, *Y*-intercept, and errors are reported here.

center of the polymethine chain should eventually adopt a pyramidal geometry because the symmetric resonance structure (Scheme 1d), which tends to force planarity in the ground state, does not contribute. During emission from the excited state at the pyramidal geometry, the ground-state electronic wave function should have a significantly reduced contribution from the planar resonance structure (Scheme 1d). In the absence of the resonance structure responsible for the dipole moment change, the IR144 dipole moment would not change until the planar geometry is attained by relaxation *after* emission. This accounts for the almost nonpolar solvatochromism of the emission maxima. Refining the zero-order hypothesis that the absorption spectra of IR144 represent that of HDITCP plus polar shifts and broadening, this suggests the shape of the steady-

TABLE 8: Exponential Decay Parameters for HDITCP in Different Solvents, Recovered from Magic-Angle Pump−Probe Experiments

solvent	A_1	τ_1 (ps)	A_2	τ_2 (ps)	A_3	τ_3 (ps)
methanol	0.19	1.71	0.08	12.3	1	412
ethanol	0.17	2.59	0.12	22.5	1	516
1-butanol	0.16	4.57	0.17	56.3	1	601
acetonitrile	0.18	2.16			1	790
propylene carbonate	0.19	2.73	0.14	24.8	1	725

TABLE 9: Exponential Decay Parameters for IR144 in Different Solvents, Recovered from Magic-Angle Pump−Probe Experiments[a]

solvent	A_1	τ_1 (ps)	A_2	τ_2 (ps)	A_3	τ_3 (ps)
methanol	0.34 (0.21)	2.30 (1.47)	0.27 (0.37)	19.0 (9.47)	1 (1)	445 (433)
ethanol	0.33 (0.21)	3.31 (2.03)	0.37 (0.43)	36.9 (19.9)	1 (1)	550 (521)
1-butanol	0.26 (0.14)	5.51 (3.20)	0.37 (0.34)	81 (36)	1 (1)	627 (565)
acetonitrile	0.41 (0.56)	4.29 (2.23)			1 (1)	804 (786)
propylene carbonate	0.42	4.24	0.33	46.1	1	807

[a] Parameters in parentheses are from fits that constrained the two fastest picosecond decay times (τ_1 and τ_2) to match three pulse echo peak shift decay constants from ref 8.

state IR144 emission spectrum should differ from that for HDITCP due to the vibrational displacements involved in the pyramidalization. The shape of the IR144 emission spectrum, which is very similar to that of HDITCP but slightly broader, could then be used to determine these displacements. On this hypothesis, the polar solvent reorganization energy λ at the planar geometry differs from half the polar solvent contribution to the observed Stokes shift. The dynamical implication of this hypothesis is that the pyramidalization will send the polar solvent reorganization energy nearly to zero.

The significantly better fit to the polarizable solute model for solvatochromism developed by McRae[45] suggests that self-consistent feedback between solute polarizability and solvent orientational polarization accounts for about half of the solvation energy. A controversial parameter in this theory is the assumed ratio $\phi = 1/2$ in $\alpha = \phi a^3$ (Onsager used $\phi = (n^2 - 1)/(n^2 + 2)$, where n is the refractive index of pure solute).[25] To gauge the extent of this feedback, ϕ was varied to find the best fit (at $\phi = 0.50$) and rough error bar ($\delta\phi = \pm 0.23$ doubled the fit error). Assuming $\phi = (n^2 - 1)/(n^2 + 2)$ and using the limiting low-frequency IR144 refractive index of $n = 1.6$ calculated from the free induction decay phase shift[87] yields $\phi = 0.34$. Ignoring issues of how to assess solute cavity size and shape in a continuum treatment, it appears that solute/reaction field feedback accounts for one-third to one-half of the polar solvent stabilization of IR144.

Excited-State Population Lifetime and Ground-State Recovery. The slowest decay in Tables 8 and 9 represents the population lifetime. The lifetimes are an order of magnitude too fast to represent radiative decay,[88] so it is likely that they represent internal conversion to the ground state. The trend in lifetimes across solvents is the same in both dyes, with IR144 lifetimes always slightly (12−82 ps) longer than those of HDITCP. The standard mechanism for such internal conversion involves a trans → cis twist in the polymethine chain[75,89] that has been extensively studied in the dicarbocyanine dye DODCI[90,91] and measured in the tricarbocyanine dye HITCI.[92] From the photoisomerization kinetics of bridged and sterically hindered tricarbocyanine dyes, it has been suggested that the twist occurs about the bond labeled bc in Scheme 1, which remains unhindered in IR144.[93] Compared to HDITCP, the slightly longer IR144 lifetimes suggest slight frictional or steric hindrance of this mechanism. For IR144 in ethanol, the pump−probe signals decay to near zero with the same lifetime (550 ps) as the excited-state absorption at 471 nm (540 ps)[84] and in rough agreement with a lifetime from phase-shift fluorometry (590 ps).[85]

For IR144 in alcohols, the magic-angle pump−probe lifetimes can be used to estimate rotational reorientation times by comparison to parallel polarization transient grating decay times.[8] Using lifetimes $L = \tau_3$ from Table 9 and adjusting the reorientation times R in the parallel transient grating signal[8]

$$S_{TG||}(T) = \exp(-2T/L)[1 + (8/5)\exp(-T/R) + (16/25)\exp(-2T/R)] \quad \text{(ref 94)}$$

to match transient grating single-exponential decay times (τ_4 in Table 2 of ref 8) yields best fit reorientation times $R = 210$ ps (methanol), 470 ps (ethanol), and 380 ps (butanol). Reorientation times more than 20% different from these values do not fit the transient grating decays within the noise. The reorientation time in methanol is reasonable in comparison to that for the dye HITCI (∼200 ps).[79,91] The methanol and ethanol reorientation times match the ratio of viscosities within error. Both the transient grating decay time and the recovered reorientation time in butanol seem anomalous.

If a long-lived ground-state isomer is formed by internal conversion from the excited state, the ground-state absorption loss amplitude will not decay to zero, but to the product of the isomerization yield and the fractional isomer/normal absorption. In both DODCI and HITCI,[92] the ground-state isomer is formed with ∼10% yield and decays on a 0.1−1 ms time scale. Since excited-state stimulated emission and loss of ground-state absorption each contribute roughly half the signal, a 10% isomer yield with no isomer absorption within the probe spectrum would imply a long-lived background with an amplitude of 0.05 relative to the lifetime. Any isomer absorption within the laser probe spectrum would decrease this background amplitude. Good fits do not require a constant background term, but the data do not extend over a few lifetimes. Inclusion of a constant background term yields amplitudes between ±0.03 relative to lifetime for different solvents, so a 10% ground-state photoisomer yield appears consistent with the data.

HDITCP Dynamics. Since the electronic polarizability response of the solvent gives rise only to an instantaneous frequency shift, any solvent response probed in HDITCP and IR125 should be essentially a mechanical response to changes in solute size upon electronic excitation. It is not possible to rigorously separate this solvent response and relaxation from

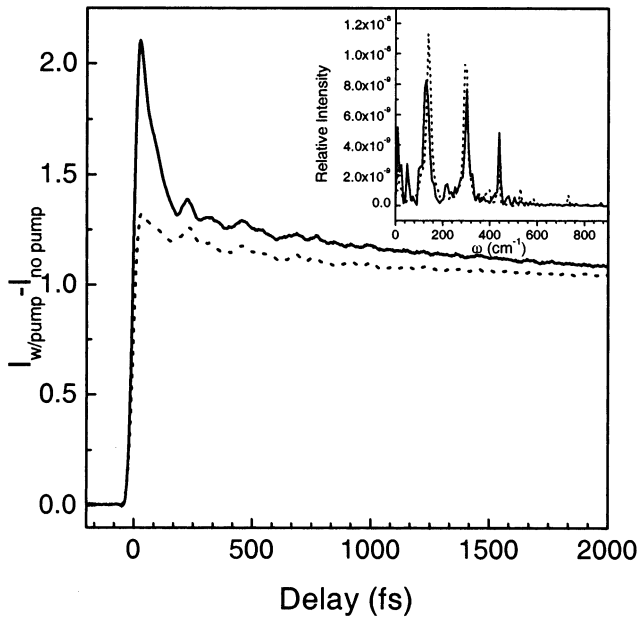

Figure 5. Magic-angle pump−probe transients of HDITCP (dotted line) and IR144 (solid line) in methanol. The plots are normalized to the same lifetime amplitude. The inset is the Fourier transform power spectra of HDITCP (dotted line) and IR144 (solid line).

the intramolecular vibrational response and relaxation (including twisting of the polymethine chain), but the solvent changes the observed relaxation significantly. The standard model for such responses is viscoelastic theory.[13] Naphthalene has an ∼60 cm^{-1} viscoelastic Stokes shift in several solvents,[18] and anthracene has an ∼200 cm^{-1} viscoelastic Stokes shift in benzyl alcohol.[95] This suggests that a significant fraction of the HDITCP response could be viscoelastic. If one assumes the diffusional amplitude is the same as for anthracene in benzyl alcohol ($f = 0.7$), one can use eq 4 and Table 2 of ref 95 to roughly estimate the diffusional viscoelastic relaxation times for methanol (2.4 ps), acetonitrile (1.3 ps), and propylene carbonate (4.4 ps). Adjustments could allow agreement with the fastest decays in Table 8, but it is also likely that vibrational relaxation and dephasing play a significant role in the observed 1−5 ps decay, especially since the times are similar to the vibrational dephasing times observed in the quantum beat decay (1−5 ps). This quantum beat decay is sensitive to homogeneous vibrational dephasing[96] but insensitive to electronic inhomogeneity.[97] Since the addition of sinusoidal functions with a distribution of frequencies causes the oscillations to decay, the quantum beat decay also reflects inhomogeneity of the vibrational frequencies (e.g., from cross-anharmonicity[98]). Inhomogeneous shifts with a 2−10 cm^{-1} wide distribution across the thermal populated states could account for the 1−5 ps quantum beat decay. Higher order nonlinear spectroscopy[99−101] is needed to distinguish homogeneous and inhomogeneous vibrational dephasing. It has been argued that vibrational population relaxation is significantly slower than vibrational dephasing in HDITCP.[80] This suggests that the intermediate relaxation (τ_2 in Table 8) represents vibrational population relaxation (including structural relaxation such as chain twisting as a special case). The 14 200 cm^{-1} band in the HDITCP fluorescence spectrum is 4−6 times less intense in acetonitrile, which does not show an intermediate decay time, suggesting a connection between this band and the intermediate HDITCP relaxation.

IR144 Dynamics. For IR144, there are two new relaxation processes to consider: pyramidalization and dielectric relaxation. The only picosecond spectral relaxation of IR144 in acetonitrile ($\tau_1 = 4.29$ ps from Table 9) represents an upper limit for the pyramidalization time scale in acetonitrile. If pyramidalization requires large amplitude piperazine motion, the pyramidalization rate should be inversely proportional to viscosity.[91] Assuming a rate inversely proportional to viscosity and $\tau_P = 1/k_P = 4.29$ ps in acetonitrile would yield $\tau_1 \leq \tau_P \leq \tau_2$ in the other solvents. Pyramidalization might be more rapid if it is a forced motion along a coordinate similar to the boat−chair interconversion of cyclohexane. Any polymethine twisting dynamics are likely to be slowed relative to HDITCP by the central ring structure in IR144.

For IR144, the slowest spectral relaxation times (τ_2 in Table 9) roughly match picosecond polar solvation times measured with a variety of solutes.[3] Because the slowest spectral relaxation in pump−probe matches the frequency−frequency correlation function $M(t)$,[35] the slowest spectral relaxation time scales can be sensibly compared to dielectric continuum predictions for solvation. For a polarizable point dipole in a spherical cavity with $\alpha = (1/2)a^3$, $M(t)$ relaxes with the longitudinal relaxation time

$$\tau_L = \left(\frac{\epsilon_\infty + 2}{\epsilon_s + 2}\right)\tau_D$$

where τ_D is the Debye relaxation time, ϵ_∞ is the infinite frequency dielectric constant, and ϵ_s is the static dielectric constant.[53] The slowest phase of alcohol solvation typically matches the longitudinal dielectric relaxation time τ_L,[3,5] and the longitudinal dielectric relaxation times are 9 ps for methanol and 77 ps for propanol. The biexponential fit parameters are in reasonable agreement with multiexponential fits to the time-dependent Stokes shift of Coumarin 153 in alcohols.[5] The picosecond relaxation in IR144 thus correlates strongly with measurements of polar solvation using other solute probes and simulations. Although the exact times depend on the details of the charge redistribution, molecular dynamics simulations consistently find that methanol has approximately biexponential solvation decay on the picosecond time scale,[102] in agreement with multiexponential dielectric relaxation for alcohols.[102] Propylene carbonate typically has a solvation time constant of (3−5) × ($\tau_L = 8$ ps) ≈ 24−40 ps, while the dielectric relaxation of propylene carbonate is almost single exponential with a dominant $\tau_D \simeq 43$ ps.[103] The solvation time constant of acetonitrile is typically (2−5) × ($\tau_L = 0.2$ ps) ≈ 0.4−1.0 ps,[3] compared to a single dielectric relaxation time $\tau_D \simeq 3.4$ ps.[104] The slowest IR144 relaxation in both acetonitrile and propylene carbonate is similar to the Debye relaxation time and is much slower than the longitudinal relaxation time. From a molecular point of view (the formal positive and negative charge in IR144 are separated by ∼8 Å, compared to solvent size of ∼3 Å), one might argue that the charge rearrangement in IR144 is closer to a pair of macroscopic electrodes (Debye relaxation) than a point dipole (longitudinal relaxation) so that a Debye relaxation is not unreasonable. Alternatively, the slower decays found for IR144 in acetonitrile (4 ps) and propylene carbonate (46 ps) are missing in Coumarin 153,[5] consistent with assignment to vibrational population relaxation.

Comparison between Polar and Nonpolar Solvation. A precise determination of the polar solvation time scales and energetics requires a careful comparison between IR144 and HDITCP. This comparison reveals a striking trend: every relaxation process in HDITCP has a larger amplitude and a larger decay time in IR144. Based on the error bars from fitting HDITCP Stokes shift vs $F_{1/2}(D,n)$, one might argue that

HDITCP could have a sensitivity to polar solvation with up to ~200 cm^{-1} Stokes shift. Estimation of the dipole change in HITCI suggests a much smaller residual polar Stokes shift of ~40 cm^{-1}.[86] However, cyanines with nonpolar solvatochromism could be sensitive to orientational solvent polarity through the exchange solvent coordinate introduced by Kim and Hynes[105] for a transition between delocalized symmetric and antisymmetric states. This theory also predicts narrowed emission spectra relative to absorption. The linear solvatochromism places an ~200 cm^{-1} upper limit on the Stokes shift for the exchange solvent coordinate. With this hypothesis, the difference in time scales between HDITCP and IR144 must be attributed to the details of the charge rearrangement or to accompanying vibrational relaxation. In any event, the more strongly polar relaxation is always slower.

There have been several discussions of the strong coupling between polar and mechanical parts of the inertial solvent response.[20−22] On longer time scales, both rotational diffusion (hence dielectric relaxation) and translational diffusion (hence shear relaxation) are inversely proportional to viscosity.[17] Molecular dynamics simulations have predicted that the solvent relaxation slows as the solute dipole moment increases,[20,21] in qualitative agreement with the observed trend from HDITCP to IR144. Assuming a viscoelastic response in HDITCP and a dielectric response in IR144 would suggest that the two responses are strongly coupled on all time scales in polar solvents. In the harmonic spectral density picture underlying $M(t)$,[20] this might be a question of the coupling spectrum rather than the spectrum of modes. Physically, an outward propagating relaxation might be apparently complete for short-range nonpolar solvation on a faster time scale than for long-range polar solvation. Such strong coupling has been suggested[15] based on the general difficulty in distinguishing polar and mechanical solvation.[18] A theory of the static cage relaxation energy would be valuable for untangling the relaxation dynamics of HDITCP. Even if the processes observed in HDITCP cannot be fully disentangled, the additional dynamics seen in IR144 can be used to characterize the polar solvation dynamics.

Some aspects of the data are inconsistent with the standard multimode Brownian oscillator model: most obviously the differences between absorption and emission widths. Although it is possible to fit the one-dimensional (1D) pump−probe data for HDITCP with a Brownian oscillator model, such 1D models cannot incorporate this difference. These models also incorporate a fixed relationship between vibrational population and vibrational dephasing time scales. In preliminary fitting, we have found that a Brownian oscillator model cannot fit both two-dimensional Fourier transform (2D FT) electronic spectra[106] and the 1D pump−probe data in methanol, but that the data sets can be simultaneously fit if pump−probe amplitude of ~0.08 is assumed to carry no reorganization energy.[81] This would suggest: (1) this amplitude represents changes in width that differ between absorption and emission; (2) the time scales of vibrational dephasing and vibrational population relaxation are separate so that some vibrational reorganization energy is effectively double-counted by modeling both time scales in the pump−probe data with Brownian oscillators; or (3) the lifetime is not a single exponential.

VI. Conclusions

The solvatochromism and relaxation dynamics of three structurally related tricarbocyanine dyes (HDITCP, IR125, and IR144) in solution were compared using absorption, fluorescence, and femtosecond magic-angle pump−probe experiments. In solvents where the conductivity indicated complete ionic dissociation, HDITCP and IR125 show classic nonpolar solvatochromism, while IR144 shows polar solvatochromism which can be attributed to a dipole moment decrease caused by the piperazine functional group. The fast relaxation dynamics of IR144 is thus expected to include vibrational and nonpolar solvation dynamics similar to HDITCP or IR125, but modified by polar solvation dynamics. Pyramidalization of the piperazine nitrogen attached to the polymethine chain of IR144 is expected to produce vibrational shifts of the spectrum and reduce or eliminate the sensitivity to polar solvation processes. This difference between IR144 and other cyanines explains why echo measurements on most cyanines[32,33] could be modeled exclusively in terms of vibrational wave packet spreading while IR144 experiments were interpreted in term of polar solvation.[11,12] The solvatochromic fit results suggest that one-third to one-half of the IR144 solvation energy arises from self-consistent feedback between the solvent reaction field and the polarizable solute. Although such large solute polarizability effects have been questioned,[47] significant feedback is supported by the IR144 refractive index calculated from the free induction decay phase shift.[87] The large refractive index at zero frequency is caused by the strong IR144 charge resonance transition in the visible.

The magic-angle pump−probe transients show that the underdamped intramolecular vibrational quantum beats (amplitudes and frequencies) are quite similar in all three tricarbocyanine dyes. The biggest difference is a fast (~100 fs) solvent-dependent "coherence spike" observed near $T = 0$ in IR144 but not in HDITCP or IR125. This spike is attributed to the femtosecond polar solvation response, which is present only in IR144 because only IR144 has a dipole moment change upon electronic excitation. The amplitude of the spike increases with the reorganization energy for decay of $M(t)$ on the same time scale.[35] The assignment of this response as "inertial" is supported by the time scale and the femtosecond two-dimensional Fourier transform electronic spectra.[81] The picosecond exponential decays attributed to solvation dynamics and/or vibrational relaxation all have slower time constants and larger amplitudes for IR144 (polar solvation) than HDITCP (nonpolar solvation). Such a relationship is not obvious if polar and nonpolar solvent responses are assumed to arise from independent additive processes. A relationship is expected if both processes are limited by the same molecular motions in every solvent (e.g., the collisions underlying viscosity).[17] More fundamentally, it has been argued that mechanical and dielectric solvent responses have a strongly coupled effect on the equilibrium solvent distribution so that the presence of one modifies the other even on the fastest time scales.[21] The observation that the polar response is uniformly slower than the nonpolar response agrees with expectations for dielectric and mechanical friction.[21] It is clear that vibrational relaxation, solvent responses to changes in solute size, and dielectric relaxation in response to change in solute charge distribution all occur simultaneously and on similar time scales. Under these circumstances, comparison between structurally related molecules with polar and nonpolar solvent responses provides an approach to measuring the change in solvation dynamics caused by charge redistribution.

Acknowledgment. We thank both anonymous referees for useful criticism. Richard Shoemaker of the Departmental NMR facility recorded the NMR spectra and assisted with their interpretation. We thank Kathy Rowlen for loaning the Raman notch filter. Casey Hynes and Hyung Kim provided stimulating discussions of continuum solvation theories and pyramidalization. We thank Kevin Lehmann, Mark Berg, and Dor Ben-

Amotz for helpful discussions of nonpolar solvation. This work was supported by grants from the Alfred P. Sloan and National Science Foundations.

References and Notes

(1) Amos, A. T.; Burrows, B. L. *Adv. Quantum Chem.* **1973**, *7*, 289−313.
(2) Rossky, P. J.; Simon, J. D. *Nature* **1994**, *370*, 263−269.
(3) Maroncelli, M.; MacInnis, J.; Fleming, G. R. *Science* **1989**, *243*, 1674−1681.
(4) McHale, J. L. *Acc. Chem. Res.* **2001**, *34*, 265−272.
(5) Horng, M. L.; Gardecki, J. A.; Papazyan, A.; Maroncelli, M. *J. Phys. Chem.* **1995**, *99*, 17311−17337.
(6) Maroncelli, M.; Fleming, G. R. *J. Chem. Phys.* **1987**, *86*, 6221−6239.
(7) Fleming, G. R.; Passino, S. A.; Nagasawa, Y. *Philos. Trans. R. Soc. London, Ser. A* **1998**, *356*, 389−404.
(8) Joo, T.; Jia, Y.; Yu, J.-Y.; Lang, M. J.; Fleming, G. R. *J. Chem. Phys.* **1996**, *104*, 6089−6108.
(9) Nagasawa, Y.; Passino, S. A.; Joo, T.; Fleming, G. R. *J. Chem. Phys.* **1997**, *106*, 4840−4852.
(10) Nagasawa, Y.; Yu, J.-Y.; Fleming, G. R. *J. Chem. Phys.* **1998**, *109*, 6175−6183.
(11) Passino, S. A.; Nagasawa, Y.; Joo, T.; Fleming, G. R. *J. Phys. Chem. A* **1997**, *101*, 725−731.
(12) Passino, S. A.; Nagasawa, Y.; Fleming, G. R. *J. Chem. Phys.* **1997**, *107*, 6094−6108.
(13) Berg, M. *J. Phys. Chem. A* **1998**, *102*, 17−30.
(14) Hubble, H. W.; Tianshu, L.; Berg, M. A. *J. Chem. Phys.* **2001**, *114*, 3662−3673.
(15) Ma, J.; Bout, D. V.; Berg, M. *J. Chem. Phys.* **1995**, *103*, 9146−9160.
(16) Richert, R. *J. Chem. Phys.* **2000**, *113*, 8404−8429.
(17) Stickel, F.; Fischer, E. W.; Richert, R. *J. Chem. Phys.* **1996**, *104*, 2043−2055.
(18) Wendt, H.; Richert, R. *J. Phys. Chem. A* **1998**, *102*, 5775−5781.
(19) Vöhringer, P.; Westervelt, R. A.; Arnett, D. C.; Feldstein, M. J.; Scherer, N. F. *J. Raman Spectrosc.* **1995**, *26*, 535−551.
(20) Ladanyi, B.; Stratt, R. *J. Phys. Chem.* **1996**, *100*, 1266−1282.
(21) Kumar, P. V.; Maroncelli, M. *J. Chem. Phys.* **2000**, *112*, 5370−5381.
(22) Tran, V.; Schwartz, B. J. *J. Phys. Chem. B* **1999**, *103*, 5570−5580.
(23) Bayliss, N. S. *J. Chem. Phys.* **1950**, *18*, 292−296.
(24) Bayliss, N. S.; McRae, E. G. *J. Phys. Chem.* **1954**, *58*, 1002−1006.
(25) Onsager, L. *J. Am. Chem. Soc.* **1936**, *58*, 1486−1493.
(26) Mataga, N.; Kubota, T. *Molecular Interactions of Electronic Spectra*; Marcel Dekker: New York, 1970.
(27) Liptay, W. In *Excited States*; Lim, E. C., Ed.; Academic Press: New York, 1974; Vol. I, pp 129−229.
(28) Larsen, D.; Ohta, K.; Fleming, G. *J. Chem. Phys.* **1999**, *111*, 8970−8979.
(29) Dorairaj, S.; Kim, H. J. *J. Phys. Chem. A* **2002**, *106*, 2322−2327.
(30) West, W.; Geddes, A. L. *J. Phys. Chem.* **1964**, *68*, 837−847.
(31) Cong, P.; Yan, Y. J.; Deuel, H. P.; Simon, J. D. *J. Chem. Phys.* **1994**, *100*, 7855−7866.
(32) Yang, T.-S.; Vöhringer, P.; Arnett, D. C.; Scherer, N. F. *J. Chem. Phys.* **1995**, *103*, 8346−8359.
(33) de Boeij, W. P.; Pshenichnikov, M. S.; Wiersma, D. A. *Chem. Phys.* **1998**, *233*, 287−309.
(34) Zhang, Y. H.; Berg, M. A. *J. Chem. Phys.* **2001**, *115*, 4223−4230.
(35) Farrow, D. A.; Yu, A.; Jonas, D. M. Manuscript in preparation.
(36) Brackmann, U. *Lambdachrome Laser Dyes*; Lambda Physik: Gottingen, 1986.
(37) Pauling, L. In *Organic Chemistry, An Advance Treatise*; Gilman, H., Ed.; John Wiley & Sons: New York, 1938; Vol. 2, pp 1850−1890.
(38) Mulliken, R. S. *J. Chem. Phys.* **1939**, *7*, 364−373.
(39) Mulliken, R. S. *J. Chem. Phys.* **1939**, *7*, 570−572.
(40) Fabian, J.; Hartmann, H. *J. Mol. Struct.* **1975**, *27*, 67−78.
(41) Reichardt, C. *Solvents and Solvent Effects in Organic Chemistry*, 2nd ed.; VCH Verlagsgesellschaft: Weinheim, Germany, 1988.
(42) Radeglia, R.; Engelhardt, G.; Lippmaa, E.; Pehk, T.; Nolte, K.-D.; Dahne, S. *Org. Magn. Reson.* **1972**, *4*, 571−576.
(43) Ooshika, Y. *J. Phys. Soc. Jpn.* **1954**, *9*, 594−602.
(44) Lippert, V. E. *Z. Naturforsch., A* **1955**, *10a*, 541−545.
(45) McRae, E. G. *J. Phys. Chem.* **1957**, *61*, 562−572.
(46) Lippert, V. E. *Z. Elektrochem.* **1957**, *61*, 962−975.
(47) Suppan, P. *Chem. Phys. Lett.* **1983**, *94*, 272−275.
(48) This discussion ignores coupling between the orientational and electronic polarization. This is justified if an enhanced electronic polarization arises through the orientational polarization as in Onsager's reaction field because this will relax with the orientational polarization. It has been argued that a large orientational polarization suppresses the electronic polarization, and another ad hoc separation has been proposed. Brady, J. E.; Carr, P. W. *J. Phys. Chem.* **1985**, *89*, 5759−5766.
(49) Marcus, R. A. *J. Chem. Phys.* **1965**, *43*, 1261−1274.
(50) Kinoshita, S.; Nishi, N. *J. Chem. Phys.* **1988**, *89*, 6612−6622.
(51) Kjaer, A. M.; Ulstrup, J. *J. Am. Chem. Soc.* **1986**, *109*, 1934−1942.
(52) Loring, R. F.; Yan, Y. J.; Mukamel, S. *J. Chem. Phys.* **1987**, *87*, 5840−5857.
(53) van der Zwan, G.; Hynes, J. T. *J. Phys. Chem.* **1985**, *89*, 4181−4188. There is a typographical error for an equation in the text between eq B.2 and eq B.3. The solute polarizability, α, should be related to the cavity radius, a, by $\alpha = [(n^2 - 1)/(n^2 + 2)]a^3$. $\alpha = (1/2)a^3$ implies either a solute refractive index $n = 2$ or a cavity volume less than the volume per molecule of the solute condensed phase (for $n < 2$).
(54) Longuet-Higgins, H. C.; Pople, J. A. *J. Chem. Phys.* **1958**, *27*, 192−194.
(55) Feynman, R. P.; Leighton, R. B.; Sands, M. *The Feynman Lectures on Physics*; Addison-Wesley: Reading, MA, 1977.
(56) Bayliss, N. S.; Rees, A. L. G. *J. Chem. Phys.* **1940**, *8*, 377−381.
(57) Rees, A. L. G. *J. Chem. Phys.* **1940**, *8*, 429−430.
(58) Nowak, R.; Bernstein, E. R. *J. Chem. Phys.* **1986**, *86*, 3197−3206.
(59) Ben-Amotz, D.; Herschbach, D. R. *J. Phys. Chem.* **1993**, *97*, 2295−2306.
(60) Kosower, E. M. *J. Am. Chem. Soc.* **1958**, *80*, 3253.
(61) Bagchi, B.; Oxtoby, D. W.; Fleming, G. R. *Chem. Phys.* **1984**, *86*, 257−267.
(62) Tolbert, C. A. M.S. Thesis, University of Colorado, Boulder, 2000.
(63) Mishra, A.; Behera, R. K.; Behera, P. K.; Mishra, B. K.; Behera, G. B. *Chem. Rev.* **2000**, *100*, 1973−2011.
(64) Tatiklov, A. S.; Shvedova, L. A.; Derevyanko, N. A.; Ischenko, A. A.; Kuzmin, V. A. *Chem. Phys. Lett.* **1992**, *190*, 291−297.
(65) This conductance meter did not allow measurements at sufficiently low concentration to determine the limiting molar conductivity at zero concentration. The *apparent* molar conductivity was determined from the change in conductivity divided by the total dye concentration. All of the neat solvents exceeded the literature conductivity, probably due to impurities.
(66) Weast, R. C. *CRC Handbook of Chemistry and Physics*, 1st student ed.; CRC Press Inc.: Boca Raton, FL, 1988. (Refractive indices were taken from the tabulation of "physical constants of organic compounds".)
(67) $\Lambda_m^0 = (Fe/6\pi)(r_+ + r_-)/r_+r_-$, where F is Faraday's constant, e is the electron charge, and r_+ (r_-) is the radius of the cation (anion). Atkins, P. *Physical Chemistry*, 5th ed.; W. H. Freeman and Company: New York, 1994.
(68) Nakahara, M.; Ibuki, K. *J. Phys. Chem.* **1986**, *90*, 3026−3030.
(69) Balbuena, P. B.; Johnston, K. P.; Rossky, P. J.; Hyun, J.-K. *J. Phys. Chem. B* **1998**, *102*, 3806−3814.
(70) West, W.; Pearce, S.; Grum, F. *J. Phys. Chem.* **1967**, *71*, 1316−1326.
(71) Sanders, J. K. M.; Hunter, B. K. *Modern NMR Spectroscopy*: *A Guide for Chemists*; Oxford University Press: Oxford, 1987.
(72) Gutowsky, H. S.; Karplus, M.; Grant, D. M. *J. Chem. Phys.* **1959**, *31*, 1278−1289.
(73) Atkins, P. W. *Physical Chemistry*, 6th ed.; W. H. Freeman and Company: New York, 1998.
(74) Henrichs, P. M.; Gross, S. *J. Am. Chem. Soc.* **1976**, *98*, 7169−7175.
(75) Ponterini, G.; Momicchioli, F. *Chem. Phys.* **1991**, *151*, 111−126.
(76) Vranken, N.; Jordens, S.; De Belder, G.; Lor, M.; Rousseau, E.; Schweitzer, G.; Toppet, S.; Van der Auweraer, M.; De Schryver, F. C. *J. Phys. Chem. A* **2001**, *105*, 10196−10203.
(77) Birks, J. B. *Photophysics of Aromatic Molecules*; Wiley-Interscience: New York, 1970.
(78) Lakowicz, J. R. *Principles of Fluorescence Spectroscopy*; Plenum Press: New York, 1983.
(79) Jonas, D. M.; Lang, M. J.; Nagasawa, Y.; Joo, T.; Fleming, G. R. *J. Phys. Chem.* **1996**, *100*, 12660−12673.
(80) Yang, T.-S.; Chang, M.-S.; Chang, R.; Hayashi, M.; Lin, S. H.; Vöhringer, P.; Dietz, W.; Scherer, N. F. *J. Chem. Phys.* **1999**, *110*, 12070−12081.
(81) Hybl, J. D.; Yu, A.; Farrow, D. A.; Jonas, D. M. *J. Phys. Chem. A* **2002**, *106*, 7651−7654.
(82) Iwata, K.; Weaver, W. L.; Gustafson, T. L. *J. Phys. Chem.* **1992**, *96*, 10219−10224.
(83) Shang, X.; Benderskii, A. V.; Eisenthal, K. B. *J. Phys. Chem. B* **2001**, *105*, 11578−11585. Shang, X.; Benderskii, A. V.; Eisenthal, K. B. *J. Phys. Chem. B* **2001**, *105*, 11928.
(84) Meyer, Y. H.; Pittman, M.; Plaza, P. *J. Photochem. Photobiol. A: Chem.* **1998**, *114*, 1−21.
(85) Thompson, R. B.; Frisoli, J. K.; Lakowicz, J. R. *Anal. Chem.* **1992**, *64*, 2075−2078.

(86) Martini, I.; Hartland, G. V. *J. Phys. Chem.* **1996**, *100*, 19764−19770.

(87) Albrecht Ferro, A.; Hybl, J. D.; Jonas, D. M. *J. Chem. Phys.* **2001**, *114*, 4649−4656. The IR144 solute refractive index was estimated from the solution free induction decay phase shift using $n_{IR144} = n_{MeOH} + (\lim_{\omega\to 0^+}[\Delta\phi(\omega)/\omega](c/z)(N_{IR144}/N_{solution})$, where $N_{IR144} = \rho_{IR144}/m_{IR144}$ is the number density of pure IR144 and $N_{solution} = C_{IR144}N_A$ is the number density used for the free induction decay. $\Delta\phi(\omega)$ is the free induction decay phase shift, c is the speed of light, and z is the path length. ρ_{IR144} is the volume density of pure IR144 (estimated at 1 g/cm^3), m_{IR144} is the IR144 molecular mass, C_{IR144} is the IR144 molar concentration used for the free induction decay measurement in solution, and N_A is the Avogadro constant.

(88) Strickler, S. J.; Berg, R. A. *J. Chem. Phys.* **1962**, *37*, 814−822.

(89) Rullière, C. *Chem. Phys. Lett.* **1976**, *43*, 303−308.

(90) Velsko, S. P.; Waldeck, D. H.; Fleming, G. R. *J. Chem. Phys.* **1983**, *78*, 249−258.

(91) Fleming, G. R. *Chemical Applications of Ultrafast Spectroscopy*; Oxford University Press: New York, 1986.

(92) Zhu, X. R.; Harris, J. M. *Chem. Phys.* **1990**, *142*, 301−309.

(93) Shvedova, L. A.; Tatikolov, A. S.; Makin, S. M.; Ramanov, N. N.; Kuz'min, V. A. *Bull. Acad. Sci. USSR Div. Chem. Sci.* **1979**, *28*, 696−701.

(94) This parallel transient grating signal (S_{TGII}) is obtained from the square of the pump−probe signal field (integrated over t). $S_{TGII}(T) = \exp(-T/L)[1 + 2r(T)]$, where the anisotropy $r(T) = (2/5)\exp(-T/R)$ for a nondegenerate two-level system. This is a special case ($\beta/\alpha = 4/5$) of the expression used by: Phillion, D. W.; Kuizenga, D. J.; Siegman, A. E. *Appl. Phys. Lett.* **1975**, *27*, 85−87.

(95) Berg, M. A.; Zhang, Y. *J. Chem. Phys.* **2001**, *115*, 4231−4238.

(96) Haroche, S. In *High Resolution Laser Spectroscopy*; Shimoda, K., Ed.; Springer-Verlag: New York, 1976; pp 253−313.

(97) Shen, Y. R. *The Principles of Nonlinear Optics*; Wiley-Interscience: New York, 1984.

(98) The vibrational energy contains anharmonic terms $x_{ij}v_iv_j$, with anharmonicity constant x_{ij} and vibrational quantum numbers v_i and v_j for modes i and j that can generate an effectively inhomogeneous distribution of vibrational frequencies for mode i due to a thermal distribution of quantum numbers for mode j.

(99) Loring, R. F.; Mukamel, S. *J. Chem. Phys.* **1985**, *83*, 2116−2128.

(100) Astinov, V.; Kubarych, K. J.; Milne, C. J.; Miller, R. J. D. *Chem. Phys. Lett.* **2000**, *327*, 334−342.

(101) Kaufman, L. J.; Blank, D. A.; Fleming, G. R. *J. Chem. Phys.* **2001**, *114*, 2312−2331.

(102) Ladanyi, B. M.; Skaf, M. S. *Annu. Rev. Phys. Chem.* **1993**, *44*, 335−368.

(103) Barthel, J.; Bachhuber, K.; Buchner, R.; Gill, J. B.; Kleebauer, M. *Chem. Phys. Lett.* **1990**, *167*, 62−66.

(104) Barthel, J.; Kleebauer, M.; Buchner, R. *J. Solution Chem.* **1995**, *24*, 1−17.

(105) Kim, H. J.; Hynes, J. T. *J. Chem. Phys.* **1992**, *96*, 5088−5110.

(106) Hybl, J. D.; Albrecht Ferro, A.; Jonas, D. M. *J. Chem. Phys.* **2001**, *115*, 6606−6622.